International Journal of Thermophysics, Vol. 27, No. 6, November 2006 (© 2006)
DOI: 10.1007/s10765-006-0121-7

Density and Surface Tension of Liquid Ternary Ni–Cu–Fe Alloys[1]

J. Brillo,[2,3] I. Egry,[2] and T. Matsushita[4]

The density and surface tension of liquid Ni–Cu–Fe alloys have been measured over a wide temperature range, including the undercooled regime. A non-contact technique was used, consisting of an electromagnetic levitator equipped with facilities for optical densitometry and oscillating drop tensiometry. At temperatures above and below the liquidus point, the density and surface tension are linear functions of temperature. The concentration dependence of the density is significantly influenced by a third-order (ternary) parameter in the excess volume. The surface tensions are rather insensitive to substitution of the two transition metals Ni, Fe against each other and depend only on the copper concentration. By numerically solving the Butler equation, the surface tension of the ternary system can be derived from the thermodynamic potentials ^{E}G of the binary phases (Ni–Cu, Fe–Cu, Ni–Fe) alone.

KEY WORDS: density; electromagnetic levitation; excess volume; liquid metals; nickel-copper-iron alloys; surface tension.

1. INTRODUCTION

1.1. Nickel–Copper–Iron

In recent years, the Ni–Cu–Fe ternary system received some attention for its electrical and magnetic properties [1, 2]. The combination of its

[1]Paper presented at the Seventeenth European Conference on Thermophysical Properties, September 5–8, 2005, Bratislava, Slovak Republic.

[2]Deutsches Zentrum für Luft- und Raumfahrt, Institut für Raumsimulation, D-51170 Köln, Germany.

[3]To whom correspondence should be addressed. E-mail: Juergen.Brillo@dlr.de

[4]Royal Institute of Technology, Department of Materials Science and Engineering, SE-100 44 Stockholm, Sweden.

low thermal expansion and its relatively high electrical and thermal conductivity makes Ni–Cu–Fe also an interesting candidate for the development of new data storage facilities [3].

From a physical point of view, Ni–Cu–Fe is characterized by attractive interactions between the two transition metals Ni and Fe on the one hand, and repulsive interactions between Cu and Fe on the other. As a consequence for the liquid state, the metastable miscibility gap of the Cu–Fe binary phase closes gradually as nickel is added to the system [4].

The aim of the investigation presented here is to study the density and surface tension of the Ni, Cu, and Fe system in the liquid phase. Up to now, there is only a limited number of experimental data available for this system. Recently, we performed density and surface tension measurement for the binary alloys, Ni–Fe, Ni–Cu, and Cu–Fe [5–7]. Here, we report on systematic measurements on the ternary system. The method used in this work is based on the containerless technique of electromagnetic levitation, which is described in Ref. 8.

1.2. Density and Molar Volume

The density, $\rho(T)$, of a liquid metal can be considered as a linear function of temperature, T, within a limited temperature interval including the melting point [5]:

$$\rho(T) = \rho_{\mathrm{L}} + \rho_{\mathrm{T}}\,(T - T_{\mathrm{L}}) \tag{1}$$

In this equation, $\rho_{\mathrm{L}}$is the density at the liquidus temperature, T_{L}, and ρ_{T} is the temperature coefficient. Although the density is the physical property of primary interest for applications, physically it is more suitable to discuss the molar volume, V, due to its extensive nature. The molar volume V is calculated from the density as $m\rho^{-1}$, where m is the mass of one mole of substance.

For a regular ternary solution with components i, each having the bulk concentration $c_{\mathrm{i}}^{\mathrm{B}}$, V is usually written as a function of temperature and concentrations [9]:

$$V(c_1^{\mathrm{B}}, \ldots, c_3^{\mathrm{B}}, T) = \sum c_{\mathrm{i}}^{\mathrm{B}} V_{\mathrm{i}}(T) + {}^{\mathrm{E}}V(c_1^{\mathrm{B}}, \ldots, c_3^{\mathrm{B}}, T) \tag{2}$$

In this equation, V_i is the molar volume of component i, and ${}^{\mathrm{E}}V$ is the excess volume. In the case of a vanishing excess volume ${}^{\mathrm{E}}V$, Eq. (2) reduces to a simple linear combination of molar volumes V_i, which is often referred to as Vegard's law [10]. In order to describe the functional dependence of ${}^{\mathrm{E}}V$ on concentration and temperature, the following form is used [9]:

$$^{\mathrm{E}}V(c_1^{\mathrm{B}},\ldots,c_3^{\mathrm{B}},T)=\sum_{i}^{2}\sum_{j>i}^{3}c_i^{\mathrm{B}}c_j^{\mathrm{B}}\,{}^{\mathrm{E}}V_{i,j}+c_1^{\mathrm{B}}c_2^{\mathrm{B}}c_3^{\mathrm{B}}\,{}^{\mathrm{E}}V^{\mathrm{T}} \tag{3}$$

In Eq. (3), $^{\mathrm{E}}V_{i,j}$ denotes the binary interaction parameter between components i and j and $^{\mathrm{E}}V^{\mathrm{T}}$is the parameter for the ternary interaction.

1.3. Surface Tension

For a liquid ternary alloy, consisting of three elements $i = 1, 2, 3$, with corresponding surface tensions, $\gamma_i(T)$, the surface tension $\gamma_{123}(T)$ of the alloy is predicted by the Butler equation [11,12]:

$$\begin{aligned}\gamma_{123}(T)&=\gamma_1+\frac{RT}{S_1}\ln\left(\frac{1-c_2^{\mathrm{S}}-c_3^{\mathrm{S}}}{1-c_2^{\mathrm{B}}-c_3^{\mathrm{B}}}\right)\\&\quad+\frac{1}{S_1}\left\{{}^{\mathrm{E}}G_1^{\mathrm{S}}(T,c_2^{\mathrm{S}},c_3^{\mathrm{S}})-{}^{\mathrm{E}}G_1^{\mathrm{B}}(T,c_2^{\mathrm{B}},c_3^{\mathrm{B}})\right\}\\&=\gamma_2+\frac{RT}{S_2}\ln\left(\frac{c_2^{\mathrm{S}}}{c_2^{\mathrm{B}}}\right)+\frac{1}{S_2}\left\{{}^{\mathrm{E}}G_2^{\mathrm{S}}(T,c_2^{\mathrm{S}},c_3^{\mathrm{S}})-{}^{\mathrm{E}}G_2^{\mathrm{B}}(T,c_2^{\mathrm{B}},c_3^{\mathrm{B}})\right\}\\&=\gamma_3+\frac{RT}{S_3}\ln\left(\frac{c_3^{\mathrm{S}}}{c_3^{\mathrm{B}}}\right)+\frac{1}{S_3}\left\{{}^{E}G_3^{\mathrm{S}}(T,c_2^{\mathrm{S}},c_3^{\mathrm{S}})-{}^{\mathrm{E}}G_3^{\mathrm{B}}(T,c_2^{\mathrm{B}},c_3^{\mathrm{B}})\right\}\end{aligned} \tag{4}$$

where R is the universal gas constant, T is the temperature, S_i is the surface area in a monolayer of pure liquid i, c_i^{B} is the mole fraction of component i in the bulk phase, and c_i^S is the mole fraction of component i in the surface phase. $^{\mathrm{E}}G_i^{\mathrm{B}}$ denotes the partial excess Gibbs free energy in the bulk and $^{\mathrm{E}}G_i^{\mathrm{S}}$ the partial excess Gibbs free energy of component i in the surface layer.

The Butler equation is based on the assumption that the surface is a monoatomic layer and can be treated as a separate thermodynamic phase. With respect to the bulk, atoms on the surface have a reduced coordination number which lowers $|^{\mathrm{E}}G_i^{\mathrm{S}}|$. It was shown by Tanaka and Iida [11] that, apart from a constant factor 3/4, $^{\mathrm{E}}G_i^{\mathrm{S}}$ could be assumed to have the same functional form as $^{\mathrm{E}}G_i^{\mathrm{B}}$:

$$^{\mathrm{E}}G_i^{\mathrm{S}}\approx\tfrac{3}{4}\,{}^{\mathrm{E}}G_i^{\mathrm{B}} \tag{5}$$

Here i is either component 1, 2, or 3. The surface area $S_i (i = 1, 2, 3)$ is calculated from the molar volume V_i as follows [6,11]: $S_i = 1.091\ (6.02 \times 10^{23})^{1/3} V_i^{2/3}$. The partial excess Gibbs free energy $^{\mathrm{E}}G_i^{\mathrm{B}}$ is derived from the excess Gibbs free energy $^{\mathrm{E}}G$ according to the usual thermodynamic relations [9].

Equations (4) and (5) imply a rule for the calculation of the surface tension from the pure elements: if ${}^{\mathrm{E}}G$ is given, Eq. (4) can be solved numerically using the surface concentrations as unknown variables. For ${}^{\mathrm{E}}G(T, c_i^{\mathrm{B}})$ an *ansatz* similar to Eq. (3) is used [9]:

$$ {}^{\mathrm{E}}G(c_1^{\mathrm{B}}, \ldots, c_3^{\mathrm{B}}, T) = \sum_{i}^{2} \sum_{j>i}^{3} c_i^{\mathrm{B}} c_j^{\mathrm{B}} \, {}^{\mathrm{E}}G_{i,j} \tag{6} $$

In Eq. (6), ${}^{\mathrm{E}}G_{i,j}$ denotes the binary interaction parameters for components i and j. This equation is a model function for the excess free energy of a sub regular solution. The effect of any existing ternary term, $c_1 c_2 c_3^{\mathrm{E}} G^{\mathrm{T}}$, was neglected so that the Gibbs free energy of the sub regular ternary solution is determined by the energies of the binary phases only [13, 14].

The parameters ${}^{\mathrm{E}}G_{i,j}$ can be written as a function of temperature and concentration according to the Redlich–Kister form [9, 13]:

$$ {}^{\mathrm{E}}G_{i,j} = \sum_{\nu=0} {}^{\nu}L_{i,j} (c_i^B - c_j^B)^{\nu} \tag{7} $$

In Eq. (7), the parameters ${}^{\nu}L_{i,j}$ depend on temperature but not on the concentrations.

2. EXPERIMENTAL

2.1. Levitation

All experiments presented in this work were carried out in an electromagnetic levitation chamber that is described in detail in Refs. 5–8. A schematic sketch of the arrangement is shown in Fig. 1. The sample is processed under a protecting atmosphere of He/8vol%–H_2 in a levitation coil to which a current of 100 Å and approximately 250 kHz is applied. It is positioned by forces due to interactions with the inhomogeneous magnetic field and melted by eddy currents that are induced within. Temperature control is achieved by cooling the sample in a laminar flow of the He/H_2 gas mixture. The temperature, T, is measured using an infrared pyrometer aimed at the top of the sample. For each sample, it is necessary to recalibrate the temperature with respect to the liquidus temperature, T_{L}. Values for T_{L} were obtained from calculations [14] based on the Calphad approach [15]. If $T_{\mathrm{P}}$is the output signal from the pyrometer, then the real temperature T is obtained using the following approximation derived from Wien's law:

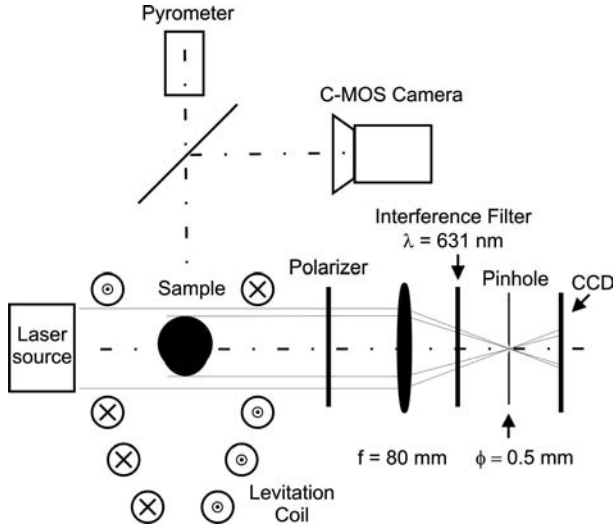

Fig. 1. Schematic diagram of the experimental arrangement.

$$\frac{1}{T}-\frac{1}{T_{\mathrm{P}}}=\frac{1}{T_{\mathrm{L}}}-\frac{1}{T_{\mathrm{L,P}}} \tag{8}$$

In Eq. (8), $T_{\mathrm{L,P}}$ is the pyrometer signal at the liquidus temperature. Equation (8) is valid only if the sample emissivity at the operating wavelength of the pyrometer $\varepsilon_{\lambda}(T)$ remains constant over the experimentally scanned range of temperature. This is a good approximation for most metals [16].

The uncertainty of the experimentally determined temperatures is generally estimated to be no larger than $\pm 20\,\mathrm{K}$. The accuracy of the Calphad calculation strongly depends on the quality of modeling and the input parameters used. For good modeling the error should be less than the typical experimental error [14]. In order to verify this, we performed a spot check measurement using a thermocouple on a $Ni_{25}Cu_{40}Fe_{35}$ sample. The obtained difference for the calculated liquidus temperature was only 6 K for this sample.

2.2. Density and Volume

To measure the density based on the volume of the sample, shadowgraphs are taken from the levitated sample. As schematically shown in Fig. 1, a polarized HeNe laser beam, equipped with a spatial filter and a

beam expander, is used to illuminate the sample from behind. The shadow image is captured by means of a digital CCD camera and analyzed by an edge detection algorithm that locates the edge curve $R(\varphi)$ where R and φ are the radius and azimuthal angle with respect to the drop center. In order to eliminate the influence of oscillations, the edge curve is averaged over 1000 frames. It is then fitted by Legendre polynomials of order$\leqslant$6;

$$\langle R(\varphi)\rangle = \sum_{i=0}^{6} a_i P_i(\cos(\varphi)) \tag{9}$$

with P_i being the i-th Legendre polynomial. As shown by an analysis of top view images [7], the equilibrium shape of the sample is symmetric with respect to the vertical axis. Hence, its volume is calculated using the following integral:

$$V_{\mathrm{P}} = \tfrac{2}{3}\pi \int_0^{\pi} < R(\varphi) >^3 \sin(\varphi)\mathrm{d}\varphi \tag{10}$$

V_{p} is the volume in pixel units. It is related to the real volume V according to $V = qV_{\mathrm{P}}$, with q being the scaling factor. The scaling factor q of the system is determined by a calibration procedure described in Ref. 7. When M is the mass of the sample, the density, ρ, is calculated from $\rho = M/V$. The uncertainty $\Delta V/V \approx \Delta\rho/\rho$ is estimated to be $\pm 1.5\%$

2.3. Surface Tension

Surface tension measurements were performed using the oscillating drop technique [8]. A fast recording C-MOS video camera (400 frames/s, 1024×1000 pixels) is directed at the sample from the top. A series of 4196 frames is recorded at each temperature and is analyzed afterwards by an edge detection algorithm. The frequency spectrum of the radius R exhibits a set of five peaks ω_m , $m = -2, -1, 0, 1, 2$, which correspond to the surface Rayleigh-oscillation modes. The surface tension is calculated from these frequencies following the sum rule of Cummings and Blackburn [17];

$$\gamma = \frac{3M}{160\pi} \sum\nolimits_{m=-2}^{+2} \omega_m^2 - 1.9\Omega^2 - 0.3\left(\frac{g}{a}\right)^2 \Omega^{-2} \tag{11}$$

where M is the mass of the sample, g is the acceleration of gravity, and a is the radius of the sample. Ω is calculated from the three translational frequencies ω_{X}, ω_{Y}, and ω_{Z} of the samples, i. e.,

$$\Omega^2 = \frac{1}{3}\left(\omega_X^2 + \omega_Y^2 + \omega_Z^2\right) \tag{12}$$

This method is attached with an uncertainty of $\Delta\gamma/\gamma \approx 5\%$. A more detailed description of this procedure is given, for instance, in Ref. 18.

2.4. Sample Composition

Two sections through the ternary system, designated in Fig. 2 as "A" and "B", were investigated. Samples along section A have concentrations according to $Ni_{0.4(1-x)}Cu_xFe_{0.6(1-x)}$. This section was chosen, because, along this cut, the binary contributions to the excess volume cancel each other as can be calculated by Eq. (3) using parameters from Table I. Along section A, the excess volume is due entirely to the ternary term.

In Section B, the copper concentration is kept constant at 20 at% and the main parameter is the concentration of nickel, which ranges from 0 to 80 at%. Section B is orthogonal to section A and is described by

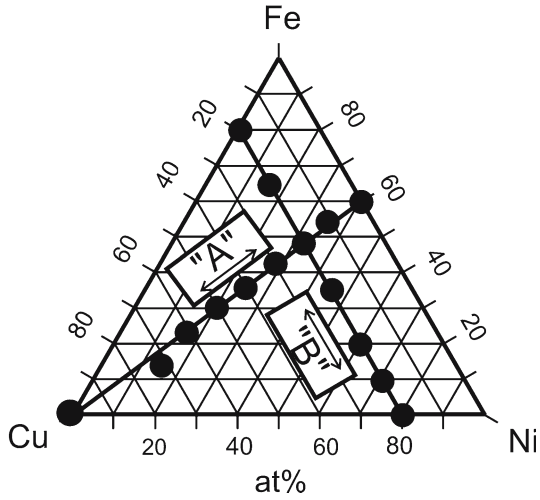

Fig. 2. Concentrations of the investigated samples. Along section A, the concentration of copper is the main parameter and the ratio of c_{Ni}^B:c_{Fe}^B is approximately 40:60. Along section B, the concentration of copper is kept constant at 20 at% and the main parameter is c_{Ni}^B which ranges from 0 to 80 at%.

Table I. Parameters ${}^{E}V_{i,j}$ for the Fe–Ni, Cu–Ni, and Cu–Fe Binary Systems from Ref. 5

System i, j	${}^{E}V_{i,j}$ ($cm^3 \cdot mol^{-1}$)
Fe, Ni	0
Cu, Ni	−0.85
Cu, Fe	+0.6

$Ni_xCu_{0.2}Fe_{0.8-x}$. The individual compositions of the investigated samples are shown as dots in Fig. 2.

3. RESULTS AND DISCUSSION

3.1. Density and Volume

Measured density values are shown in Fig. 3 for samples along section B. It is found that at temperatures, T, above and below the corresponding liquidus point, the density, $\rho(T)$, as a function of temperature can be described by a linear relation according to Eq. (1).

From these data the molar volume, V, was calculated. Its concentration dependence was studied at $T = 1773$ K, and the result is depicted in Fig. 4

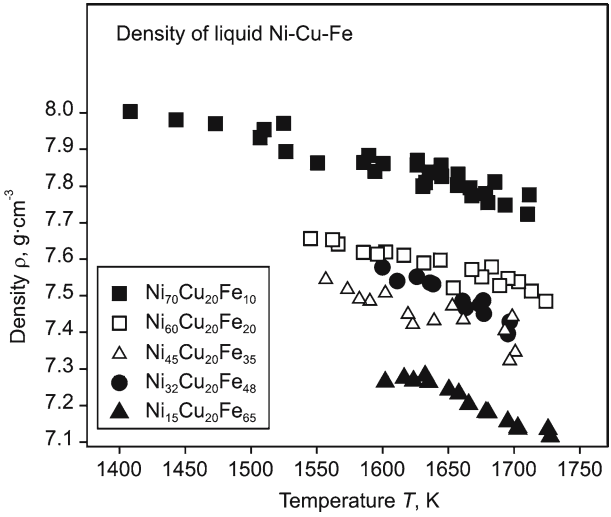

Fig. 3. Density of liquid Ni–Cu–Fe samples from section B versus temperature.

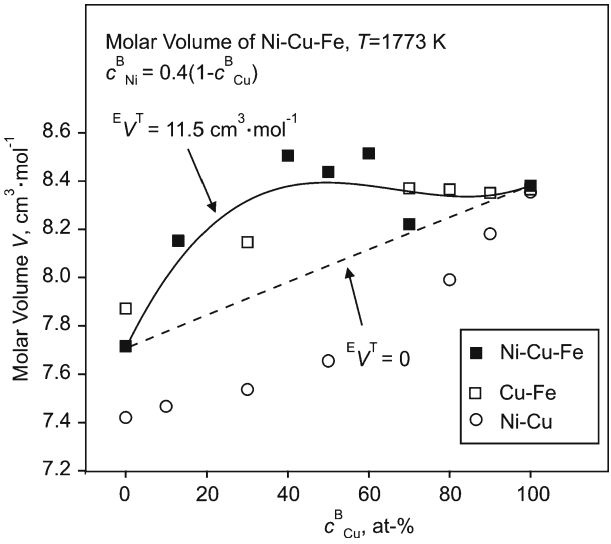

Fig. 4. Molar volume, V, of Ni–Cu–Fe samples from section A at 1773 K. The data are shown in comparison to experimental data for Cu–Fe, Ni–Cu [5] and the corresponding solutions of Eq. (3) assuming ${}^{\mathrm{E}}V^{\mathrm{T}} = 0$ (dashed line). The solid line corresponds to a fit of Eq. (3) with ${}^{\mathrm{E}}V^{\mathrm{T}} = 11.5\,\mathrm{cm}^3\cdot\mathrm{mol}^{-1}$. The concentrations of the sample with $c^{\mathrm{B}}_{\mathrm{Cu}} \approx 70$ at% lie in Fig. 2 a little off the straight line. Its volume is therefore slightly larger than expected from Eq. (3).

for section A and in Fig. 5 for section B. Starting in Fig. 4 with $Ni_{40}Fe_{60}$, the molar volume increases nearly linearly from a value of $7.7\,\mathrm{cm}^3$ up to 8.4–$8.5\,\mathrm{cm}^3$, as the copper concentration is altered to approximately 40 at%. On further increase of the copper concentration, the molar volume remains almost constant until the value of pure copper, i.e., $7.4\,\mathrm{cm}^3$, is reached. In Fig. 4, the data are shown in comparison with the molar volumes obtained for the binary systems, Cu–Fe and Cu–Ni [5]. It is noticeable that, along section A, the values of the ternary alloy seem to follow those of Cu–Fe rather than those of Cu–Ni. This seems to indicate that, upon adding nickel to Cu–Fe, the volume is maintained as long as the nickel concentration is not too large. This hypothesis is supported by the data of section B shown in Fig. 5. As long as $c^{\mathrm{B}}_{\mathrm{Ni}}$ is smaller than 50 at%, the molar volume remains at a high level of 8.0–$8.2\,\mathrm{cm}^3$ which can be seen as constant with respect to the experimental error of $\Delta V/V > 1\%$. This is also indicated by the horizontal dotted line in Fig. 5. For comparison, the data of the Fe-Ni binary system are also shown.

In order to perform a quantitative analysis, V is calculated with parameters ${}^{\mathrm{E}}V_{i,j}$ from Table I using Eq. (3) with ${}^{\mathrm{E}}V^{\mathrm{T}} = 0$. The result is

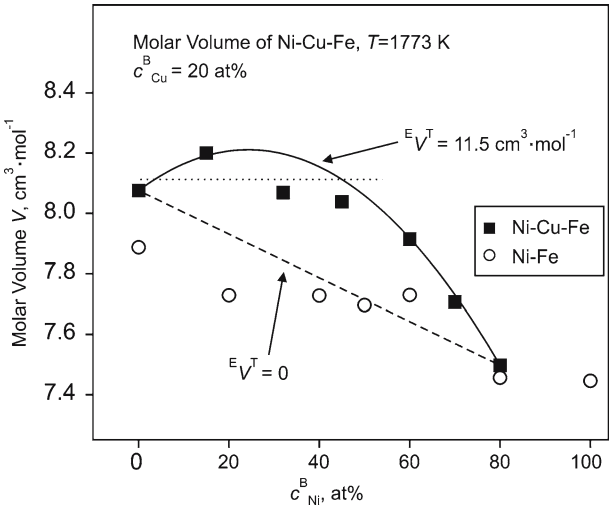

Fig. 5. Molar volumes of Ni–Cu–Fe samples from section B at 1773 K. The data are shown in comparison to the corresponding solutions of Eq. (3) assuming $^EV^T = 0$ (dashed line). The solid line is a fit of Eq. (3) with $^EV^T = 11.5\,\mathrm{cm^3 \cdot mol^{-1}}$.

shown in Figs. 4 and 5 as well. The experimental values are significantly larger indicating a positive excess volume. As mentioned above, the binary contributions to the excess volume vanish along section A, and a fit of Eq. (3) to the data can only be obtained with $^EV^T \neq 0$. The data of either section can therefore be described by Eq. (3) only, if in addition to the binary contributions, $^EV_{i,j}$, a ternary interaction parameter $^EV^T > 0$ is taken into account. A least-squares fit of Eq. (3) has been performed to all data points (Sections A and B) using $^EV^T$ as the only fit parameter. The value of $^EV^T$ obtained this way is

$$^EV^T = 11.5 \pm 1.5\,\mathrm{cm^3 \cdot mol^{-1}} \tag{13}$$

As displayed in Figs. 4 and 5, the result is in good agreement with the experimental data. As shown, $^EV^T$ is significantly higher than the interaction parameters $^EV_{i,j}$ for the binary systems. A direct numerical comparison of the interaction parameters $^EV_{i,j}$ and $^EV^T$ is difficult because these are multiplied by a different order in the concentration products $c_i c_j$ and $c_1 c_2 c_3$, respectively. The maximum contribution of the ternary parameter $^EV^T$ to the excess volume in Eq. (3) is $^EV^T/27 = 0.43\,\mathrm{cm^3 \cdot mol^{-1}}$. This value is nearly twice as much as the maximum amount of the excess

volume in Cu–Ni and nearly three times larger than the maximum excess volume in Cu–Fe.

3.2. Surface Tension

As in the case of the density, it was found that for the surface tension it could be described by a linear function of temperature, T:

$$\gamma(T) = \gamma_L + \gamma_T(T - T_L) \tag{14}$$

In this equation, $\gamma_L$is the surface tension at the liquidus temperature, T_L, and γ_T is the thermal coefficient of the surface tension $\partial\gamma/\partial T$. From the data, γ was calculated by linear interpolation at $T = 1800$ K for each concentration c^B_{Cu} in section A. The results are shown in Fig. 6.

Starting with $Ni_{40}Fe_{60}$ the surface tension decreases from 1.88–1.5 $N \cdot m^{-1}$,as the copper concentration is increased to 13 at%. For higher copper concentrations the surface tension remains almost constant at 1.2–1.3 $N \cdot m,^{-1}$which corresponds approximately to the value of pure copper. The experimental data are in good agreement with the solution of the Butler equation, Eq. (4), using the Redlich–Kister parameters from Ref. 13, as listed in Table II. The solution of the Butler equation is shown in Fig. 6 as well.

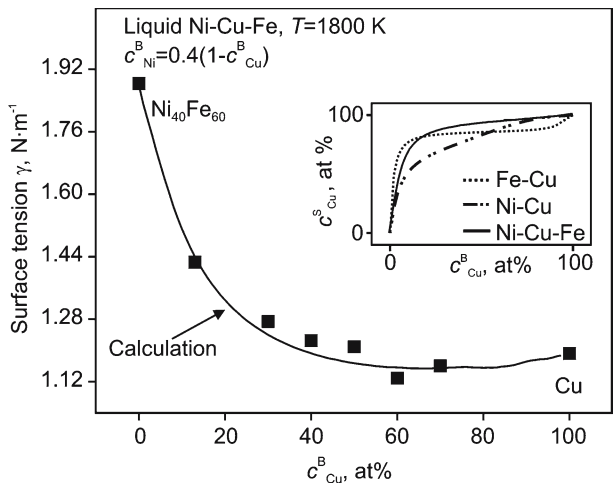

Fig. 6. Surface tension of Ni–Cu–Fe samples from section A at $T = 1800$ K versus copper concentration. The experimental data are shown in comparison to the solution of Eq. (4). The inset shows a plot of the surface concentration, c^S_{Cu}, for the ternary system in comparison to the binary phases Ni–Cu and Cu–Fe.

Table II. Interaction Parameters Used to Calculate the Excess Gibbs Free Energy ${}^{E}G$ According to Eq. (6) and (7). Parameters are Taken from Ref. 13

Parameter	Value ($J \cdot mol^{-1}$)
${}^{0}L_{Fe,Ni}$	$-18380 + 6.04T$
${}^{1}L_{Fe,Ni}$	$9228 - 3.55T$
${}^{0}L_{Cu,Ni}$	$11760 + 1.084T$
${}^{1}L_{Cu,Ni}$	-1672
${}^{0}L_{Cu,Fe}$	$36087.98 - 2.33T$
${}^{1}L_{Cu,Fe}$	$324.53 - 0.033T$
${}^{2}L_{Cu,Fe}$	$10355.39 - 3.603T$

For samples of section B, the surface tensions have also been calculated for $T = 1800\,K$. The results are shown in Fig. 7 where surface tension data are plotted versus nickel concentration, c^{B}_{Ni}. The values of the surface tension are all in a range between 1.3 and $1.45\,N \cdot m^{-1}$. The observed increase of γ with c^{B}_{Ni} is so small that it is justified to consider γ as constant in section B. Similar to the discussion of section A in Fig. 6, Fig. 7 shows the experimental data in comparison with the solution of the

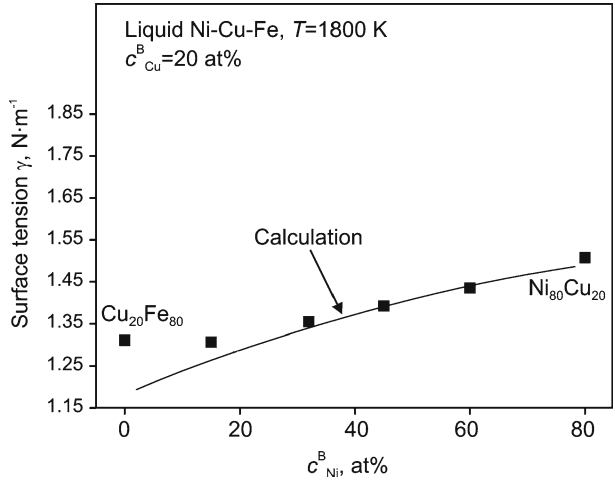

Fig. 7. Surface tension of Ni–Cu–Fe samples from section B at $T = 1800\,K$ versus nickel concentration. The experimental data are shown in comparison to the solution of Eq. (4).

Butler equation, Eq. (4), using parameters for a non-vanishing ^{E}G, taken from Ref. 13. Again, the agreement is good.

The general characteristic features of the surface segregation profiles (inset in Fig. 6) are roughly the same as for the corresponding plots for the Cu–Ni and Cu–Fe binary systems. Consequently, the surface tensions of Ni–Cu–Fe alloys should be rather insensitive to the substitution of the two transition metals Ni and Fe by each other and should depend mainly on the copper concentration. This has been confirmed by our data in Figs. 6 and 7.

4. CONCLUSIONS

The density and surface tension of liquid, undercooled Ni–Cu–Fe have been investigated systematically. For the ternary alloy, the density values cannot be derived from the properties of the binary phases alone and a large positive excess volume exists. This is different for the surface tension data, which agree well with values predicted from the Butler equation. In contrast to the density, the surface tension can be derived from the binary phases without further knowledge about the ternary system.

ACKNOWLEDGMENTS

We would like to thank R. Schmid-Fetzer for fruitful discussions and for his calculations of the liquidus temperatures used in this work. Financial support by the "Deutsche Forschungsgemeinschaft" under Grant Number EG 93/4-2 is also gratefully acknowledged.

REFERENCES

1. J. Wiggins, H. Srikanth, K.-Y. Wang, L. Spinu, and J. Tang, *J. Appl. Phys.* **87**:4810 (2000).
2. J. Binder, P. Zahn, and I. Mertig, *J. Magn. Magn. Mater.* **165**:100 (1997).
3. R. D. Cottle, X. Chen, R. K. Jain, Z. Eliezer, L. Rabenberg, and M. E. Fine, *JOM* **50**:67 (1998).
4. M. Baricco, E. Bosco, G. Acconciaioco, P. Rizzi, M. and Coisson, *Mater. Sci. Eng.* **A 375**:1019 (2004).
5. J. Brillo and I. Egry, *Z. Metallkd.* **95**:691 (2004).
6. J. Brillo and I. Egry, *Proc. High Temp. Capillarity Conf.* 2004 (*J. Mater. Sci.* **40**:2213 (2005).
7. J. Brillo and I. Egry, *Int. J. Thermophys.* **24**:1155 (2003).
8. D. M. Herlach, R. F. Cochrane, I. Egry, H. J. Fecht, and A. L. Greer, *Int. Mater. Rev.* **38**:273 (1993).
9. C. Lüdecke and D. Lüdecke, *Thermodynamik* (Springer, Heidelberg, 2000), p. 506
10. L. Vegard, *Z. Phys.* **5**:17 (1921).
11. T. Tanaka and T. Iida, *Steel Res.* **65**:21 (1994).
12. J. A. V. Butler, *Proc. Roy. Soc.* **135A**:348 (1932).

13. C. Servant, B. Sundman, and O. Lyon, *Calphad* **25**:79 (2001).
14. R. S. Schmid-Fetzer, Private Communication, TU-Clausthal, Institut f. Metallurgie, D-38678 Clausthal-Zellerfeld, Germany (2005).
15. R. S. Schmid-Fetzer and J. Gröbner, *Adv. Eng. Mater.* **3**:947 (2001).
16. S. Krishnan, G. P. Hansen, R. H. Hauge, and J. L. Margrave, *High Temp. Sci.* **29**:17 (1990).
17. D. L. Cummings and D. A. Blackburn, *J. Fluid Mech.* **224**:395 (1991).
18. S. Schneider, I. Egry, and I. Seyhan, *Int. J. Thermophys.* **23**:1241 (2002).